Swarthmore College

Works

4-1-2014

N-Methylmesoporphyrin IX Fluorescence As A Reporter Of Strand Orientation In Guanine Quadruplexes

Navin C. Sabharwal , '14

V. Savikhin

Joshua R. Turek-Herman , '16

John Michael Nicoludis , '12

V. A. Szalai

See next page for additional authors

Follow this and additional works at: https://works.swarthmore.edu/fac-chemistry

Part of the Inorganic Chemistry Commons

Let us know how access to these works benefits you

Recommended Citation

Navin C. Sabharwal , '14; V. Savikhin; Joshua R. Turek-Herman , '16; John Michael Nicoludis , '12; V. A. Szalai; and Liliya A. Yatsunyk. (2014). "N-Methylmesoporphyrin IX Fluorescence As A Reporter Of Strand Orientation In Guanine Quadruplexes". *FEBS Journal*. Volume 281, Issue 7. 1726-1737. DOI: 10.1111/febs.12734
https://works.swarthmore.edu/fac-chemistry/26

Authors

Navin C. Sabharwal , '14; V. Savikhin; Joshua R. Turek-Herman , '16; John Michael Nicoludis , '12; V. A. Szalai; and Liliya A. Yatsunyk

N-methylmesoporphyrin IX fluorescence as a reporter of strand orientation in guanine quadruplexes

Navin C. Sabharwal[1], Victoria Savikhin[2,*], Joshua R. Turek-Herman[1], John M. Nicoludis[1,†], Veronika A. Szalai[2] and Liliya A.Yatsunyk[1]

1 Department of Chemistry and Biochemistry, Swarthmore College, PA, USA
2 Center for Nanoscale Science & Technology, National Institute of Standards & Technology, Gaithersburg, MD, USA

Correspondence

L. A. Yatsunyk, Department of Chemistry and Biochemistry, Swarthmore College, 500 College Ave., Swarthmore, PA 19081, USA
Fax: +1 610 328 7355
Tel: +1 610 328 8558
E-mail: lyatsun1@swarthmore.edu
V. A. Szalai, Center for Nanoscale Science and Technology, National Institute of Standards and Technology, 100 Bureau Drive, Gaithersburg, MD 20899, USA
Fax: +1 301 975 2303
Tel: +1 301 975 3792
E-mail: Veronika.Szalai@NIST.gov

Present addresses *Department of Electrical Engineering, Stanford University, Stanford, CA, USA
†Department of Chemistry and Chemical Biology, Harvard University, Cambridge, MA,USA

Guanine quadruplexes (GQ) are four-stranded DNA structures formed by guanine-rich DNA sequences. The formation of GQs inhibits cancer cell growth, although the detection of GQs in vivo has proven difficult, in part because of their structural diversity. The development of GQ-selective fluorescent reporters would enhance our ability to quantify the number and location of GQs, ultimately advancing biological studies of quadruplex relevance and function. N-methylmesoporphyrin IX (NMM) interacts selectively with parallel-stranded GQs; in addition, its fluorescence is sensitive to the presence of DNA, making this ligand a possible candidate for a quadruplex probe. In the present study, we investigated the effect of DNA secondary structure on NMM fluorescence. We found that NMM fluorescence increases by about 60-fold in the presence of parallel-stranded GQs and by about 40-fold in the presence of hybrid GQs. Antiparallel GQs lead to lower than 10-fold increases in NMM fluorescence. Single-stranded DNA, duplex, or i-motif, induce no change in NMM fluorescence. We conclude that NMM shows promise as a 'turn-on' fluorescent probe for detecting quadruplex structures, as well as for differentiating them on the basis of strand orientation.

Introduction

DNA adopts numerous secondary structures in addition to the canonical Watson–Crick duplex. One example is G-quadruplex (GQ) DNA, a structure formed by π-π stacking of G-quartets, composed of four guanines held together by Hoogsteen hydrogen bonds [1–3] (Fig. 1). To form GQs, a DNA sequence must contain one or more regions of contiguous guanines, typically three or more. Monovalent cations, such as
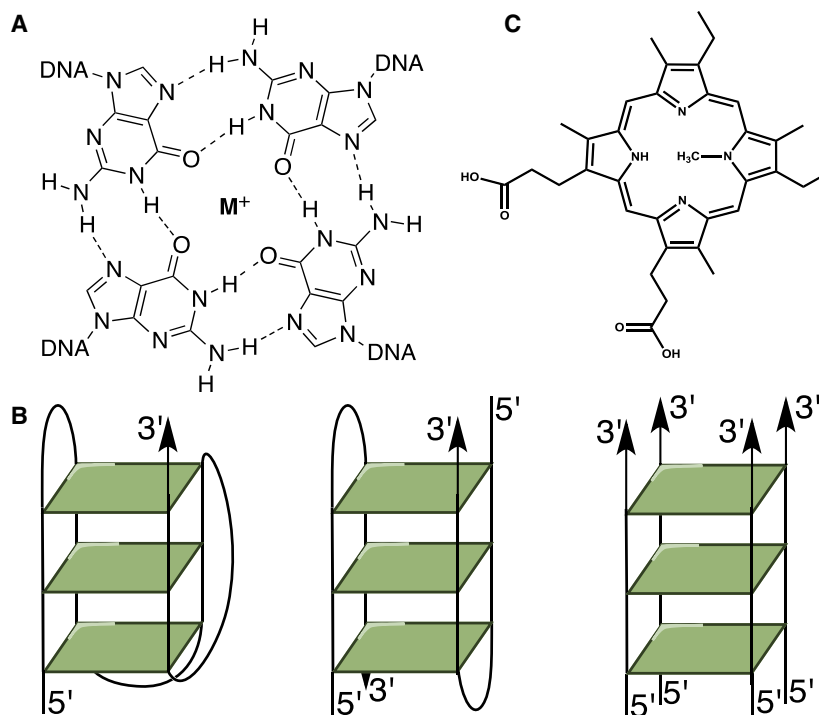
Fig. 1. Structures of GQ and NMM. (A) Structure of a G-tetrad. (B) Schematic representations of mixed-hybrid monomolecular GQ (left), antiparallel bimolecular GQ (middle) and tetramolecular parallel-stranded GQ (right). (C) Structure of NMM. Note that commercially available NMM is a mixture of four regioisomers that differ in the position of the N-Me group (only one isomer is shown); each isomer forms a pair of enantiomers with the N-Me group pointing up or down.

sodium, potassium or ammonium, stabilize GQ structures [1,4]. GQs can be uni-, bi- or tetramolecular and adopt parallel, antiparallel, or mixed-hybrid topology (Fig. 1B), depending on DNA composition, stabilizing cation and the presence of exogenous ligands [5–9].

G-rich DNA sequences with a propensity to form GQs have been identified throughout the human genome, including in telomeres, oncogenes (*c-MYC, c-MYB, c-FOS, c-ABL*), ribosomal DNA and immunoglobin switch regions [10–15]. GQs have been proposed to regulate gene expression, chromosomal alignment, recombination and DNA replication [16]. Conclusive correlation of GQs with cellular processes, however, has proved challenging, partly as a result of the structural diversity exhibited by GQs, and also because the available probes can induce GQ formation or alter their structures, making it unclear whether the GQs observed *in vivo* are present prior to probe addition. Accordingly, there is a need for new probes to clarify the physiological relevance of GQ DNA.

Selective quadruplex targeting and detection are both important and challenging. A variety of small-molecule probes display fluorescence that is modulated by the presence of GQs; such molecules are highlighted in a recent review [17]. The majority of these probes suffer from low selectivity for GQ versus double-stranded DNA (dsDNA) or toward a specific GQ geometry. It is important to discriminate GQs based on their geometry because it defines the biological roles and functions of

GQs, such as interactions with proteins [18] and drugs [19,20]. The first example of a 'turn-on' fluorescent small molecule dye specific for parallel-stranded (but not antiparallel or mixed-hybrid GQs) was reported recently [21]. This acetylene-bridged purine dimer (APD) interacts with a variety of parallel-stranded GQ structures, displays strong emission in their presence, and exhibits topology-specific staining in agarose gels. Its synthesis, however, is not trivial. By contrast to this small molecule example, Balasubramanian's group reported immunofluorescence detection of GQs [22], thereby improving the ability to map GQs *in vivo*. The need remains for additional GQ selective probes that are either commercially available or easy to prepare and compatible with sensitive *in vivo* detection, primarily by fluorescence microscopy.

N-methylmesoporphyrin IX (NMM) (Fig. 1C) is highly selective for GQ over single-stranded DNA (ssDNA) and ssRNA, dsDNA, triplex DNA and DNA–RNA hybrids [23,24]. Previous studies have demonstrated that NMM fluorescence increases in the presence of GQ but not dsDNA [25,26]. Recently, NMM was shown to bind parallel but not antiparallel GQs [23,27]. The potential of NMM to discriminate between particular strand orientations of GQs using fluorescence, however, has not been systematically explored. NMM is water-soluble, chemically stable, and commercially available molecule with excellent optical and fluorescence properties. These attributes,

combined with the ability of NMM to preferentially recognize parallel-stranded GQ structures, make it a promising candidate for selective GQ detection. In the present study, we applied UV-visible, fluorescence and CD spectroscopies to evaluate the potential of NMM as a selective fluorescence GQ reporter in the presence of a wide selection of DNA structures.

Results and Discussion

In light of the exceptional selectivity of NMM for GQ DNA relative to other DNA secondary structures [24,25] and the unique ability of this ligand to discriminate between parallel versus antiparallel GQ conformation [23], we aimed to determine whether NMM could

be used as a GQ-specific fluorescence probe. To achieve this goal, we measured the fluorescence of NMM in the presence of a variety of DNA sequences and secondary structures, including ssDNA, dsDNA and i-motif DNA, as well as carefully selected GQ DNA with representative folding topologies (Table 1). GQ secondary structures are usually defined as follows. Mixed-hybrid quadruplexes contain one strand running in the opposite direction from the other three strands (Fig. 1B, left). Antiparallel GQs contain two strands that run in opposite direction from the two remaining strands; for example, the bimolecular GQ shown in Fig. 1B (middle). A parallel-stranded GQ has all four DNA strands running in the same direction, as shown in Fig. 1B (right), for a tetramolecular GQ. The secondary struc-

Table 1. Oligonucleotide conformation and fluorescence enhancement and lifetime data.

Name	Conformation[a]		Fluorescence enhancement[b]	Fluorescence lifetimes (τ_1; ns)[c]
	Without NMM	With NMM		
C1A	ss	ss	0.69 ± 0.19 (TB)	
Tel22, 100Li	ss	ss	1.22 ± 0.21 (100Li)	
CT	ds	ds	0.00 ± 0.05	
			0.03 ± 0.07 (50Na)	
ds26	ds	ds	0.25 ± 0.06	
C1A:C1B	ds	ds	0.44 ± 0.22 (TB)	
C8	i	i	1.25 ± 0.65 (5K 5.8)	
i-cMyc	i	i	1.53 ± 0.12 (5K 5.8)	
$C_4T_4C_4$	i	i	0.45 ± 0.16 (5K 5.8)	
TC_4T	i	i	0.44 ± 0.00 (5K 5.8)	
IL1	P	P	55.7 ± 6.8 (TB)	
G4	P	P	67.8 ± 4.3	7.83 ± 0.01
			65 ± 11 (TB)	8.29 ± 0.01 in TB
G8	P	P	69.9 ± 3.7	8.00 ± 0.01
			57.5 ± 4.2 (TB)	7.97 ± 0.01 in TB
VEGF	P	P	52.9 ± 2.0	7.09 ± 0.01
cMyc	P	P	64.8 ± 3.8	7.96 ± 0.01
cKit2	P	P	46.3 ± 1.6	6.35 ± 0.01
cKit1	P/M	P	41.9 ± 2.5	
G4TERT	P/M	P	50.2 ± 6.1	
Bcl-2	P/M	P	47.9 ± 1.2	
Tel22	M	P	25.5 ± 2.4	τ_1 = 7.26 ± 0.02 (89)
				τ_2 = 2.00 ± 0.03 (11)
26TelG4	A/M	M	34.1 ± 4.6	
$G_4T_4G_4$	A/M	M	60.2 ± 4.6	7.13 ± 0.01
Tel22, 50Na	A	A	1.59 ± 0.18	τ_1 = 5.18 ± 0.01 (60 ± 2)
				τ_2 = 0.68 ± 0.002 (40 ± 2)
TBA	A	A	15.5 ± 1.4	τ_1 = 5.81 ± 0.01 (90 ± 4)
				τ_2 = 1.07 ± 0.01 (10 ± 4)
TBA, 50Na	A	A	5.15 ± 0.39	
26TelG4, 50Na	A	A	12.1 ± 1.3	
$G_4T_4G_4$, 50Na	A	A/M	16.0 ± 1.1	τ_1 = 6.85 ± 0.002 (88 ± 3)
				τ_2 = 1.34 ± 0.01 (12 ± 3)

[a] A, antiparallel; ds, double-stranded (duplex); I, i-motif; M, mixed; P, parallel; ss, single-stranded. [b] Buffer is 5K unless specified otherwise.
[c] Population is given in parenthesis as a percentage and is 100% if not specified.

ture of each DNA in the present study was verified using CD spectroscopy (Figs S1 and S2).

Quadruplex sequences chosen in the present study include oncogene promoters, telomeric DNA and some synthetic sequences. Specifically, Tel22 [28] and 26TelG4 are human telomeric DNA sequences; $G_4T_4G_4$ is telomeric DNA from the ciliate *Oxytricha nova*. This latter sequence was chosen because it maintains antiparallel topology both in potassium [29] and sodium [30] buffers. G4TERT corresponds to a DNA sequence in the promoter of hTERT, a catalytic domain of telomerase [31]. Oncogene promoters tested in the present study include VEGF, Bcl-2, cKit and cMyc. VEGF is an oncogene promoter for vascular endothelial growth factor that is upregulated in a variety of cancers [14]; Bcl-2 inhibits cell apoptosis in B-cell lymphoma cancer cell lines [32]; cKit is a tyrosine kinase receptor that controls cell growth [33]; and cMyc is a transcriptional regulator of approximately 15% of human genes involved in a variety of cancers [34]. In addition, we tested nonphysiological DNA sequences that are models for GQs. The thrombin-binding aptamer (TBA) [35] was used in the present study because, similar to $G_4T_4G_4$, it forms an antiparallel topology regardless of buffer condition; G4 and G8 always form simple homogeneous tetramolecular parallel quadruplexes; and IL1 forms a parallel-stranded quadruplex with single-stranded overhangs that contain nucleotides other than thymine.

Titration of NMM with parallel and antiparallel GQs monitored by fluorescence to determine saturation limit and binding constants

NMM fluoresces weakly in aqueous solution, although its fluorescence increases dramatically in the presence of certain DNA structures [26]. Thus, NMM can serve as a 'turn-on' fluorescent probe. To determine the amount of DNA required to reach the fluorescence signal saturation point for NMM, we performed fluorescence titrations of NMM using a subset of DNA sequences. Titration data for the tetramolecular parallel quadruplexes, G4 and G8, and for the antiparallel/mixed-hybrid quadruplex $G_4T_4G_4$ are shown in Fig. 2; data for the intramolecular parallel quadruplex, VEGF, are shown in Fig. S3. These data indicate that at least five equivalents of GQ DNA are required to saturate NMM fluorescence. For consistency, 10 equivalents of DNA structural element were used per NMM molecule in all subsequent experiments.

Our titration data allowed determination of binding constants. The maximum fluorescence intensity as a function of added GQ DNA was fit to a 1:1 binding
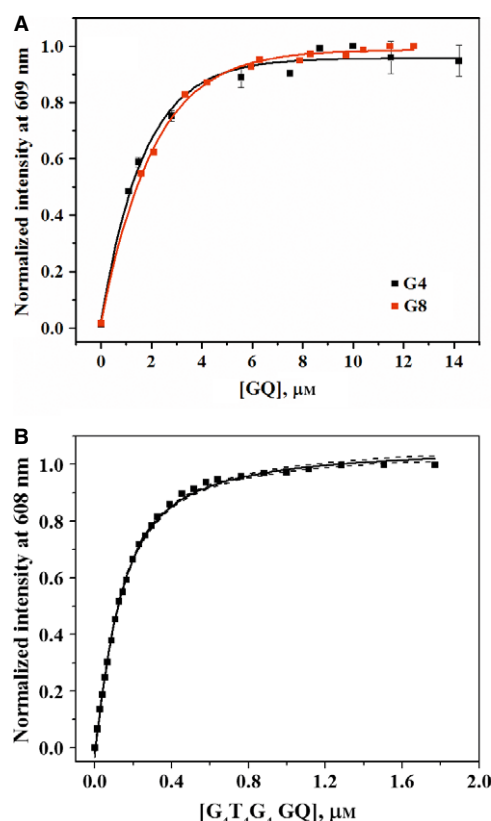

Fig. 2. Normalized fluorescence data for titration of (A) 1.0 μM NMM with G4 and G8 in TB buffer and (B) 0.1 μM NMM with $G_4T_4G_4$ in 5K buffer at 25 °C. Data for G4 and G8 are the average of three individual titrations. Solid lines represent global fits to a 1 : 1 binding model and dashed lines represent the 95% confidence interval. Binding constants were determined to be $(1.4 \pm 0.2) \times 10^6$, $(1.7 \pm 0.2) \times 10^6$ and $(1.26 \pm 0.07) \times 10^7$ L·mol^{-1} for G4, G8 and $G_4T_4G_4$, respectively. Note, the data for $G_4T_4G_4$ could be satisfactory fit to a 1 NMM : 2 GQ binding model with K_a of $(5.4 \pm 0.5) \times 10^7$ L·mol^{-1}.

model, yielding K_a of $(1.4 \pm 0.2) \times 10^6$ L·mol^{-1} for G4, $(1.7 \pm 0.2) \times 10^6$ L·mol^{-1} for G8 and $(1.1 \pm 0.1) \times 10^6$ L·mol^{-1} for VEGF. Fits improved (as judged by residuals) for VEGF when the NMM to GQ binding ratio was changed to 1:2, yielding K_a of $(7.0 \pm 0.9) \times 10^6$ L·mol^{-1}. We utilized Job plot experiments (method of continuous variation) to verify independently the stoichiometry of the NMM–VEGF interaction. Analysis of the Job plot indicates either a 1:1 or 1:2 binding stoichiometry (Fig. S3B). From these data, we conclude that one molecule of NMM binds two molecules of VEGF when VEGF is in excess, although it binds only one molecule of VEGF when concentrations of DNA and NMM are comparable.

$G_4T_4G_4$ quadruplex, which adopts an antiparallel/mixed-hybrid topology in potassium buffer, displayed

tight binding to NMM with K_a of $(1.26 \pm 0.07) \times 10^7$ L·mol^{-1} using a 1 : 1 binding model. This affinity is two orders of magnitude higher than the previously reported binding affinity of NMM to a different mixed-hybrid quadruplex, Tel22, 1.0×10^5 L·mol^{-1} [23]. Overall, the affinity of NMM for the GQ structures decreases in the order: $G_4T_4G_4$ > VEGF ≈ G8 ≈ G4 > Tel22. This ordering correlates qualitatively with higher steady-state NMM fluorescence in the presence of $G_4T_4G_4$, G4, G8 and VEGF compared to Tel22 in 5K buffer (Fig. 3). The tight binding between NMM and $G_4T_4G_4$ is somewhat unexpected. In potassium buffer, $G_4T_4G_4$ forms an antiparallel dimer [29], which would leave no room for NMM binding. Currently, our laboratory is investigating the details of this interaction to uncover possible reasons for this apparently anomalous behavior.

When NMM was titrated with predominantly antiparallel $G_4T_4G_4$ and 26TelG4, both in 50Na buffer, the fluorescence intensity increased in a linear fashion not reaching saturation even at a >16-fold excess of DNA over NMM (Fig. S4). The observed increase in fluorescence is well below that obtained for $G_4T_4G_4$ in 5K buffer. The data suggest weak and/or nonspecific binding of NMM to these sequences.

The presence of parallel GQs increases NMM steady-state fluorescence intensity and fluorescence lifetime

To establish the utility of NMM as a fluorescent probe for quadruplex detection, we determined how the fluorescence of NMM changes in the presence of a 10-fold excess of a variety of DNA structures. Figure 3 shows that ssDNA and dsDNA have little effect on NMM fluorescence in agreement with previous equilibrium dialysis experiments [24]. These same equilibrium dialysis experiments indicated significant binding between NMM and the i-motifs TC$_4$T and C$_4$T$_4$C$_4$ [24]. By contrast, we did not observe fluorescence increases in the presence of any of the i-motifs that we tested (i-cMyc, C8, TC$_4$T and C$_4$T$_4$C$_4$). This discrepancy could be a result of the difference in experimental conditions and nature of techniques utilized to observe interaction between NMM and DNA. Specifically, the buffer used in the equilibrium dialysis experiments contained 6 mM Na$_2$HPO$_4$, 2 mM NaH$_2$PO$_4$, 1 mM Na$_2$EDTA, and 185 mM NaCl (pH 7.0), whereas our buffer, 5K 5.8, had lower ionic strength, lower pH and 5 mM KCl. The insensitivity of NMM to i-motifs (at least as reported by fluorescence and UV-visible spectroscopy) emphasizes its exceptional selectivity for GQ DNA structures.

The steady-state fluorescence of NMM increases in the presence of GQ DNA. We investigated the specificity of this increase by utilizing selected G-rich oligonucleotides that adopt well-defined secondary structures, including parallel, mixed-hybrid and antiparallel (Table 1). IL1, G4, G8, cMyc, cKit2 and VEGF sequences adopt parallel-stranded topology alone or in the presence of NMM on the basis of our CD spectra ([23] and Fig. S1). The addition of a 10-fold excess of these DNA structures to NMM leads to a fluorescence enhancement of more than 50
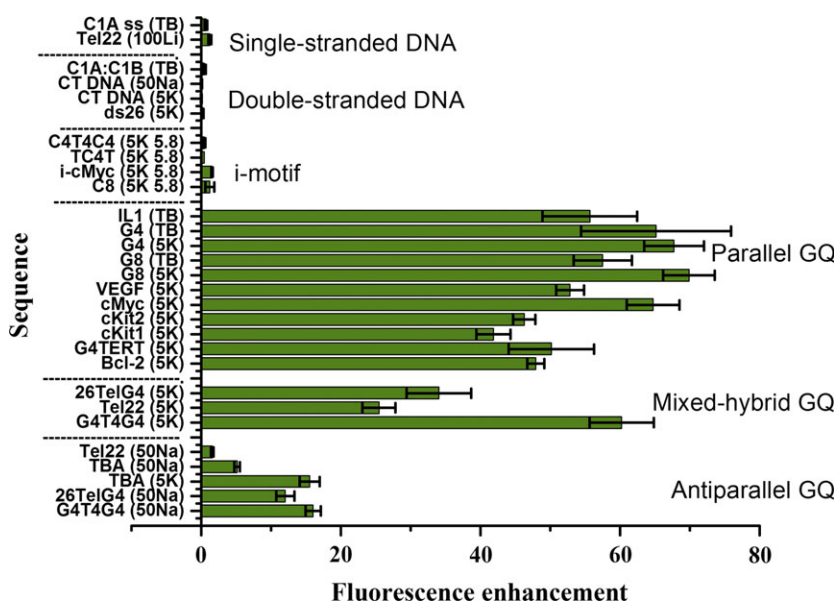

Fig. 3. Summary of steady-state fluorescence data for NMM incubated with a 10-fold molar excess of indicated sequences. Fluorescence enhancement is reported relative to the fluorescence of NMM alone. Error bars are 1 SD (confidence interval of 68.2%).

(Fig. 3 and Table 1) with the only exception being cKit2, for which fluorescence enhancement is 46. Sequences exhibiting starting parallel/mixed-hybrid conformations, such as cKit1, G4TERT and Bcl-2, generally lead to fluorescence enhancement of 42 to 50.

Sequences with predominantly mixed-hybrid GQ topology, such as Tel22 and 26TelG4 in 5K buffer, lead to a significantly smaller fluorescence enhancement of 25 and 34, respectively. As in the titration experiments, $G_4T_4G_4$ GQ in 5K buffer produces an anomalous result. This sequence adopts an antiparallel/mixed-hybrid topology (CD data; Fig. S2), yet leads to a fluorescence enhancement of 60, which is similar to that caused by parallel GQ structures. A large increase in the fluorescence of NMM upon the addition of $G_4T_4G_4$ in 10 mM HEPES buffer with 150 mM NaCl and 5 mM KCl was also reported previously [25]. A possible explanation is that NMM might convert $G_4T_4G_4$ to a structure (or a mixture) containing significant parallel component. Indeed, increased parallel component is detected by CD for this sequence under conditions of two-fold NMM excess (Fig. S2). It is important to note that the fluorescence samples contained 10-fold excess DNA (not excess NMM), leading us to expect that only a small fraction of GQ DNA could be structurally altered by NMM if it acts in a stoichiometric fashion.

Incubating NMM with predominantly antiparallel G-rich sequences resulted in only a small increase in fluorescence, the lowest of which was observed for Tel22 and TBA in 50Na, 1.6 and 5.2, respectively. Low fluorescence enhancements suggest a lack of interaction between NMM and these antiparallel structures, consistent with our previous study [23]. This interpretation is further supported by CD annealing studies in which NMM failed to induce changes in these DNA structures ([23] and Fig. S2). Other sequences in this group, $G_4T_4G_4$ and 26TelG4 in 50Na or TBA in 5K, caused small but significant increases in NMM fluorescence. These increases, however, are three- to six-fold lower than those observed for parallel GQ sequences. We tested whether NMM has an effect on the folds of these sequences by CD annealing ([23] and Fig. S2) and observed that the topologies of 26TelG4 in 50Na and TBA in 5K do not change in the presence of NMM. By contrast, the addition of NMM to $G_4T_4G_4$ in 50Na leads to an increase in the CD signal at 264 nm, consistent with an increase in parallel component of GQ structure. Our result differs from a previous study indicating that annealing of $G_4T_4G_4$ DNA with one equivalent of NMM in a buffer containing 140 mM NaCl does not change its CD signal [36]. This

discrepancy is most likely a result of the lower amount of NMM and different buffer composition used in the latter study.

The presence of a high concentration of potassium ions shifts folding equilibria toward fully-folded GQ structures with a higher parallel component. Potassium is also known to significantly stablize GQ conformations minimizing the ability of ligands to affect quadruplex topology. To test this possibility, we performed fluorescence experiments in buffer with 150 mM KCl. (Fig. S5A). Under this condition, most of the DNA sequences (cKit1, cKit2, G4TERT, Bcl-2, 26TelG4 and $G_4T_4G_4$) displayed a significant increase in CD spectral intensity at 264 nm (Fig. S5B). Overall, the data collected in 150K buffer resemble those collected in 5K buffer. Notably, all of the parallel (or predominantly parallel) sequences (G4, G4TERT, Bcl-2, Kit2, cMyc, VEGF) generate a somewhat lower enhancement of NMM fluorescence in 150K versus 5K buffer; the only exception is cKit1, which exhibits an unchanged fluorescence. The small decrease in fluorescence enhancement observed in 150K buffer could be explained by weaker binding of NMM to DNA at this increased ionic strength. By contrast, NMM in the presence of mixed-hybrid (Tel22), antiparallel (TBA) or predominantly antiparallel (26TelG4) quadruplexes showed an increase in fluorescence enhancement in 150K versus 5K buffer, as would be expected for quadruplexes with an increased parallel component. $G_4T_4G_4$ GQ once again displayed anomalous behavior characteristic of parallel GQs and not mixed-hybrid GQs. It is important to emphasize that the overall trends of fluorescence enhancement were reproducible in buffers with low or high potassium ion concentrations.

Statistical analysis of the fluorescence enhancement data confirms the unique selectivity of NMM toward GQs versus nonquadruplex structures (Table S4). For example, the fluorescence of NMM at 610 nm is 150- and 390-fold higher on average in the presence of Tel22 and G8 (in 5K) versus dsDNA, respectively. More importantly, NMM can differentiate GQ structures based on their strand orientation. The fluorescence enhancement values increase in the order: antiparallel < mixed-hybrid < parallel. The ratio of fluorescence enhancements for predominantly parallel GQs (inter- or intramolecular) versus antiparallel GQ is 5.9 and for parallel GQs versus mixed-hybrid is 2.0 when the values in each category are averaged (Table S3). In previous equilibrium dialysis experiments, a discrimination ratio of 2 was reported [24]. This ratio appears to depend on the identity of the G-rich sequences and on buffer conditions.

When different conformations of Tel22 are compared (mixed-hybrid GQ in K^+-buffer, antiparallel GQ in Na^+-buffer and predominantly single-stranded in Li^+-buffer), the preference of NMM for mixed-hybrid (or possibly parallel GQ fold) is obvious (Fig. S6). The overall discrimination pattern for NMM is similar to that of another recently reported fluorescent probe, APD [21]. However, the fluorescence of APD did not increase in the presence of Tel22, in contrast to our observation with NMM; the effect of i-motifs on APD fluorescence was not reported.

We hypothesized that the observed increase in steady-state emission of NMM in the presence of GQs is a result of protection of NMM from dynamic quenching by water. To test this idea, we collected fluorescence lifetimes for NMM in the presence of representative quadruplex topologies (Table 1). The fluorescence lifetime of NMM is the longest (6–8 ns) in the presence of predominantly parallel-stranded GQs. By contrast, NMM exhibits two lifetimes (5–7 ns and 1–2 ns) when it interacts with antiparallel or mixed-hybrid GQ structures. The key result is that the steady-state fluorescence enhancement values correlate with fluorescence lifetimes (Fig. S7A). In another experiment, we used isotopic substitution of deuterium oxide (D_2O) for water because D_2O decreases dynamic quenching of fluorophores [37]. As predicted, the steady-state fluorescence intensity of NMM in D_2O increased relative to that in H_2O (Fig. S7B). The results of these experiments are consistent with our hypothesis that binding of NMM to a quadruplex protects it from solvent, leading to increased fluorescence.

NMM fluorescence detects parallel-stranded GQs in the presence of duplex DNA

It is important that quadruplex DNA should be recognized by its probe even in the context of a large background of dsDNA. To demonstrate that NMM is capable of such selective recognition, we performed two sets of competition experiments. A solution of NMM containing > 10-fold-excess of the parallel-stranded G4 or VEGF quadruplex was titrated with increasing amounts of C1A:C1B dsDNA or genomic CT dsDNA, respectively. In both cases, the fluorescence of NMM did not change even when a 100-fold excess of dsDNA was added (Fig. S8). This is consistent with previous experiments, where we observed that the melting temperature of NMM-stabilized Tel22 did not decrease even in the presence of 480-fold excess dsDNA [23]. In a reverse competition experiment, a solution of NMM with 100-fold excess duplex was titrated with increasing amounts of either G4 or VEGF quadruplex. In both

cases, the titration data were practically indistinguishable from the titrations of NMM (alone, in the absence of duplex) with GQ (Fig. S3C for the VEGF case). The binding constants obtained for NMM–VEGF complex with or without CT DNA are within experimental error of each other $(6.9 \pm 1.5) \times 10^6$ $L \cdot mol^{-1}$ and $(7.0 \pm 0.9) \times 10^6$ $L \cdot mol^{-1}$, respectively (assuming 2 : 1 GQ : NMM binding stoichiometry).

Disruption of GQ structure decreases NMM fluorescence

Treatment of GQ structures with LiOH dissociates DNA strands. This process is driven by deprotonation of the N1 site on guanine at a pH above its pK_a of 9.4, which leads to electrostatic repulsion of the strands. We observed unfolding of G4 or IL1 GQs upon treatment with LiOH via CD spectroscopy (for IL1, see Fig. S1). When NMM was incubated with G4 or IL1, its fluorescence increased as expected but fell to levels typical for NMM alone when DNA was treated with LiOH prior to addition of NMM (Fig. S9). These results further highlight the ability of NMM to discriminate between GQ DNA and other DNA structures (single-stranded DNA in this case).

NMM fluorescence is predominantly independent of pH and buffer composition

Physiological pH varies from 7 to 9; thus, it is ideal that the potential fluorescent probe remain insensitive to changes in pH in this range. To test the sensitivity of NMM to pH, an aqueous solution of NMM was titrated either with acid (HCl) or base (NaOH). The NMM fluorescence spectrum retained its overall shape but slightly increased in intensity (by 1.5- to 2.0-fold) when the pH was increased from 2.0 to 8.6 (Fig. S10A). Upon further pH increase, a new signal emerged at 636 nm that was at least 25-fold more intense than the signal in the original spectrum (Fig. S10B). Observed pH changes were reversible because the addition of acid to a basic solution of NMM regenerated the starting NMM fluorescence spectrum (Fig. S10C). Neutralization of the acidic solution of NMM lead to a relatively small change in spectral shape and intensity (Fig. S10D).

Because working with biological molecules requires buffered solutions, we tested the fluorescence of NMM in five commonly used buffers over a wide pH range: 8.3 (Tris), 7.2 and 5.8 (lithium cacodylate), and 4.9 and 4.0 (sodium acetate). Again, NMM displayed only a small (approximately 1.3-fold) decrease in fluorescence intensity with decreasing pH (Fig. S11).

We proceeded to test the fluorescence of NMM in the presence of selected DNA sequences in two potassium-containing buffers: lithium cacodylate at pH 7.2 (5K) and Tris at pH 8.3 (TB). Direct comparison of the increase in NMM fluorescence induced by G4 and G8 reveals that the values in TB are slightly lower than in 5K: 65 ± 11 versus 68 ± 4 for G4 and 58 ± 4 versus 70 ± 4 for G8. Both measurements show, however, that NMM fluorescence increases significantly and reproducibly in the presence of parallel quadruplex, indicating that the enhancement is observed easily over a range of experimental conditions.

In short, the fluorescence of NMM is only weakly sensitive to the nature of the buffer or the pH (in the physiological pH range), making it highly suitable for biological detection of quadruplex DNA. It is important to note that the amount and type of monovalent cation, as well as solution pH, can modulate DNA structure and, therefore, any DNA interactions with NMM thereby affecting the fluorescence of NMM.

Conclusions

For use in fluorescence microscopy, a candidate dye should possess a large extinction coefficient, be selective toward its target and have an acceptable quantum yield. NMM meets the first criterion: its extinction coefficient is 1.45×10^5 M^{-1}·cm^{-1} [38] and it shows a Soret band red shift of approximately 20 nm upon DNA binding [23]. Duplex-binding dyes, such as propidium iodide, which are used routinely for fluorescence microscopy of DNA, exhibit a 20- to 30-fold increase in fluorescence when bound to DNA. NMM displays little change in fluorescence intensity in the presence of ssDNA (regardless of G-content), dsDNA or i-motif DNA, and a modest increase in fluorescence in the presence of antiparallel quadruplexes. By marked contrast, the fluorescence of NMM increases more than 40-fold upon the addition of parallel-stranded GQ DNA, making it an attractive 'light-switch' fluorescent probe. The sequence Tel22, which is a fragment of the human telomeric repeat, leads to an enhancement of 28 ± 2 fold in the fluorescence of NMM in 5K buffer (where Tel22 exist in a mixed-hybrid form) but only an enhancement of 2.6 ± 0.2 fold in 50Na buffer (where Tel22 adopts antiparallel topology) or an enhancement of 2.2 ± 0.2 fold in 100Li buffer (where Tel22 is single-stranded), indicating that discrimination of the type of fold adopted by the human telomeric sequence *in vivo* could be achieved by fluorescence microscopy of NMM-stained samples.

Materials and methods

Porphyrins, oligonucleotides and buffers

NMM was purchased from Frontier Scientific (Logan, UT, USA), dissolved in water (resistivity 1.8×10^5 Ωm) at 0.3–1.3 mM, and stored at 4 °C. NMM stock solutions were freshly diluted with appropriate buffers. NMM concentrations were determined spectrophotometrically using $\varepsilon_{379\ nm}$ = 1.45×10^5 M^{-1}·cm^{-1} [38]. Tris(hydroxymethyl)amino methane (Tris), boric acid, hydrochloric acid, cacodylic acid, lithium hydroxide (LiOH), tetramethylammonium chloride (TMACl), potassium chloride and magnesium chloride were standard grade reagents and were used as received. The DNA oligonucleotide sequences used in the present study are provided in Table S1. All oligonucleotides were purchased from commercial vendors. Selected sequences were purified by ethanol precipitation as described in the Supporting information, Doc. S1. The buffers used were:

> 10 mM lithium cacodylate (pH 7.2), 5 mM KCl, 95 mM LiCl (5K);
> 10 mM lithium cacodylate (pH 7.2), 150 mM KCl (150K);
> 10 mM lithium cacodylate (pH 5.8), 5 mM KCl, 95 mM LiCl (5K 5.8);
> 10 mM lithium cacodylate (pH 7.2), 50 mM NaCl, 50 mM LiCl (50Na);
> 10 mM lithium cacodylate (pH 7.2), 100 mM LiCl (100Li);
> 50 mM Tris-borate (pH 8.3), 10 mM KCl, 1 mM MgCl$_2$ (TB); and
> 50 mM Tris-borate (pH 8.3), 10 mM TMACl, 1 mM MgCl$_2$ (TB-TMACl).

The complete list of buffers is provided in Table S2. TMACl was used in lieu of KCl because it minimizes GQ formation [39].

To induce the formation of the most thermodynamically stable GQ conformations, oligonucleotides were diluted in the desired buffer (with or without added salts) and melted at > 90 °C for 5 min. When required, aliquots of concentrated stock solutions of KCl and/or MgCl$_2$ were mixed into the heated solution, which was then allowed to heat for an additional 5 min, cooled to room temperature over 3 h, and incubated overnight at 4 °C. The i-motif structures were formed by preparing C-rich sequences in acidic pH 5.8 [40]. For experiments testing NMM interaction with rigorously single-stranded G-rich sequences, GQs assembled from IL1 or G4 in TB buffer were treated with 50 mM LiOH for 30 min, after which the pH was adjusted to neutral by the addition of HCl. The disruption of the quadruplex into single strands was verified using CD spectroscopy.

The C1A:C1B duplex was formed in solutions containing 120 μM of each strand in TB-TMACl buffer. The solution was heated to 95 °C for 10 min, and cooled to room temperature over a period of 3 h. The final duplex was either used as

generated or gel-purified on nondenaturing PAGE using TMACl in the running buffer as described previously [41]. A dry sample of calf-thymus (CT) DNA was dissolved in 10 mM lithium cacodylate and 1 mM Na_2EDTA to a concentration of approximately 1 mM (in base pairs) and placed on a nutator for 1 week at 4 °C. Before use, the sample was centrifuged extensively to remove insoluble components and the supernatant was transferred to a clean microcentrifuge tube. Stock DNA and NMM solutions were stored at −80 °C; samples in buffers were stored at either −20 °C or 4 °C depending on the length of time between sample preparation and use.

Concentrations of all DNA samples were determined spectrophotometrically at room temperature on two types of UV-visible spectrophotometers and are reported as the concentration of structural element: GQ, i-motif or duplex. For example, the concentration of a unimolecular GQ is equal to the concentration of oligonucleotide strand, whereas the concentration of a tetramolecular GQ is assumed to be one quarter of the oligonucleotide strand concentration. The concentration of genomic CT DNA is reported in base pairs. Extinction coefficients for all single-stranded oligonucleotides are provided in Table S1 and were calculated using the nearest-neighbor approximation [42,43]. Secondary structures of all DNA sequences were verified using CD wavelength scans.

CD spectroscopy

For CD experiments, DNA samples were prepared at 1–10 μM concentrations in desired buffers. Spectra were collected on two types of CD spectropolarimeters; one of which was equipped with a Peltier temperature control unit (error of ±0.3 °C). Samples were placed in cylindrical quartz cuvettes (pathlengths of 0.1 or 0.5 cm) or a 1-cm quartz cuvette. Three scans were collected from 330 to 220 nm with a 1-nm bandwidth and an average time of 1 s at 25 °C and averaged. CD data were treated as described previously [44]. CD spectra of selected sequences were collected in the presence of a two-fold excess of NMM to determine its effect on DNA secondary structure. For these experiments, samples were annealed with or without NMM at 90 °C for 10 min, slowly cooled to room temperature and stored at 4 °C overnight before collecting CD scans.

UV-visible and fluorescence spectroscopy

UV-visible spectra for absorption titrations were collected on a spectrophotometer with a Peltier-thermostatted cuvette holder (error of ±0.3 °C) using a 1-cm quartz cuvette. Spectra were collected in the range of 350–700 nm at 25 °C. All experiments were performed at least three times on independently prepared solutions.

Fluorescence experiments were performed on three types of commercially available spectrofluorometers. An NMM solution was prepared in the desired buffer at 1 μM and its steady-state fluorescence spectrum was measured. DNA was added to NMM at 10-fold excess, the sample was equilibrated at room temperature for up to 1 h and its fluorescence spectrum was remeasured. The amount of DNA required to saturate the NMM fluorescence signal was determined from fluorescence titrations, which also were used to obtain binding constants. Titrations of 1 μM NMM were conducted with G4 (in TB), G8 (in TB) and VEGF (in 5K), all of which are parallel-stranded GQs; with antiparallel/mixed-hybrid $G_4T_4G_4$ (5K); and with antiparallel $G_4T_4G_4$ (50Na) and 26TelG4 (50Na). Spectra of NMM in the presence of G4 and G8 were collected in 100-μL volume quartz cuvettes with excitation wavelength of 399 nm, emission wavelength range from 550 to 750 nm, slits of 0.5 nm, and an integration time of 1 or 2 s. Spectra of NMM in the presence of VEGF, $G_4T_4G_4$ and 26TelG4 were collected in a 1-cm quartz cuvette using excitation wavelength of 399 nm, emission wavelength range from 550 to 700 nm, increment of 1 nm, integration time of 0.5 s, slits of 2 nm, and temperature of 25 °C. Quadruplex $G_4T_4G_4$ in 5K displays tight binding to NMM ($K_a > 10^7$ M^{-1}); in this case, a solution of only 0.1 μM NMM was titrated with the quadruplex; data were collected at a single wavelength of 608 nm using two points per second and a 50-s duration (which corresponds to 100 scans with 0.5-s integration time) to improve the signal-to-noise ratio. All data were corrected for dilution and fit to extract the association constants, K_a, as described previously [23]. Reported errors originate from the global fit of two to three collected data sets. Both, 1 NMM:1 DNA and 1 NMM:2 DNA binding models were considered. Changes in fluorescence intensity at λ_{max} (610 nm for NMM and 607–609 nm for NMM bound to DNA) are reported as fluorescence enhancement and were calculated by taking the difference between the fluorescence intensity in the presence and absence of DNA divided by the fluorescence intensity recorded for NMM alone. Uncertainties in the fluorescence intensities arise predominantly from lamp intensity variation at the excitation wavelength from day to day and errors associated with pipetting small volumes. Error bars on fluorescence enhancement values are 1 SD (confidence interval of 68.2%), derived from replicate experiments. Statistical analysis performed on the fluorescence enhancement data are provided in Tables S3 and S4 and in Doc. S2.

Competition titrations via fluorescence

To determine the selectivity of NMM for GQ structures, two sets of competition titrations were performed. In one set, a solution of 1.0 μM NMM containing approximately 10 μM of G4 or VEGF was titrated with increasing amounts of dsDNA. In another set of experiments, a solution of 1.0 μM NMM containing up to 100 μM of dsDNA was titrated with an increasing amount of G4 or VEGF. These titrations were performed at 25 °C in TB (for G4) or 5K (for VEGF) buffers.

pH studies

To measure the effect of pH on NMM fluorescence, 1–2 μM NMM in H_2O was titrated with 0.1 M of either HCl or NaOH to achieve the desired pH. The pH, fluorescence and UV-visible data were collected after each addition of acid or base. The experiments were run either as titrations or using a batch method. For fluorescence, slits were 3.5–5 nm. Titrations were repeated four times.

To test the reversibility of the NMM fluorescence as a function of pH UV-visible and fluorescence spectra of two NMM samples were recorded at neutral pH. The pH of the first sample was brought down to approximately 3.2, then back up to neutral. The pH of the second sample was brought up to approximately 10.5, then back down to neutral. The solution pH was adjusted using either 0.25 M HCl or 0.25 M LiOH. These experiments were repeated twice.

The effect of pH and buffer type on the fluorescence of NMM was tested in five buffers that contained 10 mM of Tris (pH 8.3), lithium cacodylate (pH 7.2 and 5.8) or sodium acetate (pH 4.9 and 4.0). All buffers were supplemented with 5 mM KCl and 95 mM LiCl.

Fluorescence lifetime measurements

Fluorescence lifetimes were collected for NMM in the presence of representative GQ structures on a multi-frequency cross-correlation phase and modulation fluorometer at room temperature [45,46]. Samples were prepared at concentrations of NMM ranging from 0.7 to 2.3 μM with GQ ratios ranging from 1 : 4 to 1 : 30, depending on the sequence. The excitation wavelength was 399 nm; sample emission was filtered through a 550-nm longpass filter and referenced to a scatterer with counts that were matched to that of the sample. The frequency range over which data were collected was 1–250 MHz. The number of frequencies collected varied from 10 to 50, depending on the sample. Lifetimes were calculated from fits to the phase delay and modulation ratio data as described previously using commercially available software [47]. Errors are either associated with global fits to multiple scans or are 1 SD calculated from multiple lifetime measurements for a given sample. The low fluorescence intensity of free NMM in a buffer made it impossible to measure its lifetime accurately with our instrumentation.

Acknowledgements

References

1 Williamson JR, Raghuraman MK & Cech TR (1989) Monovalent cation-induced structure of telomeric DNA: the G-quartet model. *Cell* **59**, 871–880.

2 Sen D & Gilbert W (1992) Guanine quartet structures. *Methods Enzymol* **211**, 191–199.

3 Kang C, Zhang X, Ratliff R, Moyzis R & Rich A (1992) Crystal structure of four-stranded Oxytricha telomeric DNA. *Nature* **356**, 126–131.

4 Sen D & Gilbert W (1990) A sodium-potassium switch in the formation of four-stranded G4-DNA. *Nature* **344**, 410–414.

5 Burge S, Parkinson GN, Hazel P, Todd AK & Neidle S (2006) Quadruplex DNA: sequence, topology, and structure. *Nucleic Acids Res* **34**, 5402–5415.

6 Esposito V, Galeone A, Mayol L, Oliviero G, Virgilio A & Randazzo L (2007) A topological classification of G-quadruplex structures. *Nucleosides Nucleotides Nucleic Acids* **26**, 1155–1159.

7 Li J, Correia JJ, Wang L, Trent JO & Chaires JB (2005) Not so crystal clear: the structure of the human telomere G-quadruplex in solution differs from that present in a crystal. *Nucleic Acids Res* **33**, 4649–4659.

8 Haider SM, Parkinson GN & Neidle S (2003) Structure of a G-quadruplex-ligand complex. *J Mol Biol* **326**, 117–125.

9 Parkinson GN, Lee MPH & Neidle S (2002) Crystal structure of parallel quadruplexes from human telomeric DNA. *Nature* **417**, 876–880.

10 Huppert JL & Balasubramanian S (2007) G-quadruplexes in promoters throughout the human genome. *Nucleic Acids Res* **35**, 406–413.

11 Di Antonio M, Rodriguez R & Balasubramanian S (2012) Experimental approaches to identify cellular G-quadruplex structures and functions. *Methods* **57**, 84–92.

12 Bugaut A & Balasubramanian S (2012) 5′-UTR RNA G-quadruplexes: translation regulation and targeting. *Nucleic Acids Res* **40**, 4727–4741.

13 Todd AK & Neidle S (2011) Mapping the sequences of potential guanine quadruplex motifs. *Nucleic Acids Res* **39**, 4917–4927.

14 Sun DK, Guo KX & Shin YJ (2011) Evidence of the formation of G-quadruplex structures in the promoter region of the human vascular endothelial growth factor gene. *Nucleic Acids Res* **39**, 1256–1265.

15 Mathad RI, Hatzakis E, Dai JX & Yang DZ (2011) c-MYC promoter G-quadruplex formed at the 5 '-end of NHE III1 element: insights into biological relevance and parallel-stranded G-quadruplex stability. *Nucleic Acids Res* **39**, 9023–9033.

16 Bochman ML, Paeschke K & Zakian VA (2012) DNA secondary structures: stability and function of G-quadruplex structures. *Nat Rev Genet* **13**, 770–780.

17 Vummidi BR, Alzeer J & Luedtke NW (2013) Fluorescent probes for G-quadruplex structures. *ChemBioChem* **14**, 540–558.

18 Biffi G, Tannahill D & Balasubramanian S (2012) An intramolecular G-quadruplex structure is required for binding of telomeric repeat-containing RNA to the telomeric protein TRF2. *J Am Chem Soc* **134**, 11974–11976.

19 Monchaud D & Teulade-Fichou M-P (2008) A hitchhiker's guide to G-quadruplex ligands. *Org Biomol Chem* **6**, 627–636.

20 Georgiades SN, Karim NHA, Suntharalingam K & Vilar R (2010) Interaction of metal complexes with G-quadruplex DNA. *Angew Chem Int Ed* **49**, 4020–4034.

21 Nikan M, Di Antonio M, Abecassis K, McLuckie K & Balasubramanian S (2013) An acetylene-bridged 6,8-purine dimer as a fluorescent switch-on probe for parallel G-quadruplexes. *Angew Chem Int Ed* **52**, 1428–1431.

22 Biffi G, Tannahill D, McCafferty J & Balasubramanian S (2013) Quantitative visualization of DNA G-quadruplex structures in human cells. *Nat Chem* **5**, 182–186.

23 Nicoludis JM, Barrett SP, Mergny J-L & Yatsunyk LA (2012) Interaction of human telomeric DNA with *N*-methyl mesoporphyrin IX. *Nucleic Acids Res* **40**, 5432–5447.

24 Ragazzon P & Chaires JB (2007) Use of competition dialysis in the discovery of G-quadruplex selective ligands. *Methods* **43**, 313–323.

25 Arthanari H, Basu S, Kawano TL & Bolton PH (1998) Fluorescent dyes specific for quadruplex DNA. *Nucleic Acids Res* **26**, 3724–3728.

26 Paramasivan S & Bolton PH (2008) Mix and measure fluorescence screening for selective quadruplex binders. *Nucleic Acids Res* **36**, e106.

27 Nicoludis JM, Miller ST, Jeffrey PD, Barrett SP, Rablen PR, Lawton TJ & Yatsunyk LA (2012)

28 Phan AT (2010) Human telomeric G-quadruplex: structures of DNA and RNA sequences. *FEBS J* **277**, 1107–1117.

29 Haider S, Parkinson GN & Neidle S (2002) Crystal structure of the potassium form of an *Oxytricha nova* G-quadruplex. *J Mol Biol* **320**, 189–200.

30 Schultze P, Smith FW & Feigon J (1994) Refined solution structure of the dimeric quadruplex formed from the Oxytricha telomeric oligonucleotide d (GGGGTTTTGGGG). *Structure* **2**, 221–233.

31 Lim KW, Lacroix L, Yue DJE, Lim JKC, Lim JMW & Phan AT (2010) Coexistence of two distinct G-quadruplex conformations in the hTERT promoter. *J Am Chem Soc* **132**, 12331–12342.

32 Dai J, Dexheimer TS, Chen D, Carver M, Ambrus A, Jones RA & Yang D (2006) An intramolecular G-quadruplex structure with mixed parallel/antiparallel G-strands formed in the human BCL-2 promoter region in solution. *J Am Chem Soc* **128**, 1096–1098.

33 Phan AT, Kuryavyi V, Burge S, Neidle S & Patel DJ (2007) Structure of an unprecedented G-quadruplex scaffold in the human c-kit promoter. *J Am Chem Soc* **129**, 4386–4392.

34 Gonzalez V & Hurley LH (2010) The c-MYC NHE III1: function and regulation. *Annu Rev Pharmacol Toxicol* **50**, 111–129.

35 Macaya RF, Schultze P, Smith FW, Roe JA & Feigon J (1993) Thrombin-binding DNA aptamer forms a unimolecular quadruplex structure in solution. *Proc Natl Acad Sci* **90**, 3745–3749.

36 Paramasivan S, Rujan I & Bolton PH (2007) Circular dichroism of quadruplex DNAs: applications to structure, cation effects and ligand binding. *Methods* **43**, 324–331.

37 Förster T & Rokos K (1967) A deuterium isotope solvent effect on fluorescence. *Chem Phys Lett* **1**, 279–280.

38 Ren J & Chaires JB (1999) Sequence and structural selectivity of nucleic acid binding ligands. *Biochemistry* **38**, 16067–16075.

39 Fahlman RP & Sen D (1999) 'Synapsable' DNA double helices: self-selective modules for assembling DNA superstructures. *J Am Chem Soc* **121**, 11079–11085.

40 Leroy J-L, Guéron M, Mergny J-L & Hélène C (1994) Intramolecular folding of a fragment of the cytosine-rich strand of telomeric DNA into an i-motif. *Nucleic Acids Res* **22**, 1600–1606.

41 Sambrook J & Russell D (2001) Molecular Cloning A Laboratory Manual, 3rd edn. Cold Spring Harbor Laboratory Press, Cold Spring Harbor, NY.

42 Borer PN (1975) Optical properties of nucleic acids, absorption, and circular dichroism spectra. In

Optimized end-stacking provides specificity of *N*-methyl mesoporphyrin IX for human telomeric G-quadruplex DNA. *J Am Chem Soc* **134**, 20446–20456.

Handbook of Biochemistry and Molecular Biology (Fasman G, ed.), pp. 589. CRC Press, Cleveland, OH.

43 Tataurov AV, You Y & Owczarzy R (2008) Predicting ultraviolet spectrum of single stranded and double stranded deoxyribonucleic acids. *Biophys Chem* **133**, 66–70.

44 Bhattacharjee AJ, Ahluwalia K, Taylor S, Jin O, Nicoludis JM, Buscaglia R, Brad Chaires J, Kornfilt DJP, Marquardt DGS & Yatsunyk LA (2011) Induction of G-quadruplex DNA structure by Zn(II) 5,10,15,20-tetrakis(*N*-methyl-4-pyridyl)porphyrin. *Biochimie* **93**, 1297–1309.

45 Gratton E, Alcala JR & Barbieri B (1991) Frequency domain fluorometry. Handbook of Luminescence Techniques in Chemical and Biochemical Analysis. Marcel Dekker Inc., New York, NY.

46 Lackowicz JR (2006) Principles of Fluorescence Spectroscopy, 3rd edn. Springer Science + Business Media, New York, NY.

47 Jameson DM & Gratton E (1983) Analysis of heterogeneous emissions by multifrequency phase and modulation fluorometry. In New Directions in Molecular Luminescence (Eastwood D, ed.). pp. 67–81, ASTM STP 822. American Society of Testing and Materials, Philadelphia, PA.

Supporting information

Additional supporting information may be found in the online version of this article at the publisher's web site:

Doc. S1. Ethanol precipitation.

Doc. S2. Statistical analysis of fluorescence enhancement data.

Fig. S1. CD spectra of selected DNA sequences.

Fig. S2. CD annealing studies of DNA in the presence of a two-fold excess NMM.

Fig. S3. Fluorescence titration of NMM with VEGF in 5K buffer at 25 °C.

Fig. S4. Fluorescence titration of NMM with $G_4T_4G_4$ and with 26TelG4 in 50Na buffer at 25 °C.

Fig. S5. Fluorescence enhancement and CD study in 150K buffer.

Fig. S6. Fluorescence spectra of NMM alone and with Tel22 in different buffers.

Fig. S7. NMM fluorescence intensity is modulated by dynamic solvent quenching.

Fig. S8. Competition titration of (NMM + GQ DNA) with dsDNA.

Fig. S9. Effect of LiOH on fluorescence of NMM in the presence of G4 in TB buffer.

Fig. S10. Effect of pH on the fluorescence spectra of NMM.

Fig. S11. Effect of pH and buffer type on the fluorescence spectra of NMM.

Table S1. Oligonucleotide sequences, extinction coefficients and fluorescence enhancement data.

Table S2. Composition of buffers.

Table S3. Raw data used for statistical analysis.

Table S4. Summary of *t*-test statistics for pairwise comparison.